

RSC Advances



This is an *Accepted Manuscript*, which has been through the Royal Society of Chemistry peer review process and has been accepted for publication.

Accepted Manuscripts are published online shortly after acceptance, before technical editing, formatting and proof reading. Using this free service, authors can make their results available to the community, in citable form, before we publish the edited article. This *Accepted Manuscript* will be replaced by the edited, formatted and paginated article as soon as this is available.

You can find more information about *Accepted Manuscripts* in the [Information for Authors](#).

Please note that technical editing may introduce minor changes to the text and/or graphics, which may alter content. The journal's standard [Terms & Conditions](#) and the [Ethical guidelines](#) still apply. In no event shall the Royal Society of Chemistry be held responsible for any errors or omissions in this *Accepted Manuscript* or any consequences arising from the use of any information it contains.

Directed synthesis, growth process and optical properties of monodispersed CaWO_4 microspheres via a sonochemical route

Jira Janbua¹, Jitkasem Mayamae¹, Supamas Wirunchit¹, Rattanaï Baitahe¹
and Naratip Vittayakorn^{1,2,3*}

¹Electroceramic Research Laboratory, College of Nanotechnology, King Mongkut's
Institute of Technology Ladkrabang, Bangkok 10520, Thailand

²Department of Chemistry, Faculty of Science, King Mongkut's Institute of
Technology Ladkrabang, Bangkok 10520, Thailand

³Advanced Materials Science Research Unit, Faculty of Science, King Mongkut's
Institute of Technology Ladkrabang, Bangkok 10520, Thailand

*Corresponding author. E-mail: naratipcmu@yahoo.com

Abstract

Monodispersed calcium tungstate (CaWO_4) microspheres were synthesized successfully via a sonochemical process in deionized (DI) water. The functional group and phase formation analyses were carried out using Fourier transform infrared (FT-IR) and X-ray diffraction (XRD), respectively. XRD revealed that all samples were of pure tetragonal scheelite structure. FT-IR and Raman analysis exhibited a W-O stretching peak of molecular $[\text{WO}_4]^{2-}$, which related to the scheelite structure. The effect of ultrasonic irradiation times in the sonochemical process was investigated briefly for 1, 5, 15 and 30 min. The shape of the particles was revealed as spherically monodispersed with narrow size distribution and uniform features at the ultrasonic time of 5 min. This study also found that the spherical surface was composed of tightly packed nanosphere subunits. A possible mechanism for the formation of CaWO_4 powders with a different ultrasonic time was discussed in detail. Optical

properties showed blue light emission at a wavelength of around 426 nm and an optical energy gap (E_g) value of 3.32 - 3.36 eV.

Keywords: sonochemical, monodispersed CaWO_4 microspheres, tetragonal scheelite, optical energy gap (E_g)

Introduction

The tetragonal scheelite structure and space group $I4_1/a$ of Calcium tungstate (CaWO_4) has a Ca and W ion in 8-fold, and tetrahedral site of oxygen coordination, respectively.¹ It is well known that CaWO_4 with a scheelite structure is a commercially important material with luminescence properties [1-3]. It has been used as blue phosphor (433 nm) in laser host materials [4-6,7], quantum electronics, scintillators in medical devices [1,3-5], and oscilloscopes [1,3-5]. Phosphors made up from monodispersed and microsized spherical morphology are known to be suitable for application because they have higher packing density, scattering and re-absorption of light than small spherical particles [8-10]. As a result, their high resolution, screen brightness and efficiency provide better luminescence performance.

However, an ideal morphology of phosphor particles demands a perfect spherical shape, narrow size distribution and non-agglomeration. Therefore, various preparation methods have been developed actively for controlling morphology, size and distribution. For instance, Pan *et al.* [8] synthesized quasi-monodispersed AWO_4 (A=Ca, Sr, and Ba) microspheres with a diameter of about 3 μm by a hydrothermal route at a temperature of 180 $^\circ\text{C}$ for 8 h in the presence of citric acid. Although this method uses a low reaction temperature, it has a long holding time in the synthesis process. Furthermore, monosized CaWO_4 microspheres were obtained by Zhang *et al.* [9] via a large scale solvothermal method (4.4 to 6.8 μm) with a surfactant-assisted solution route, in which either sodium

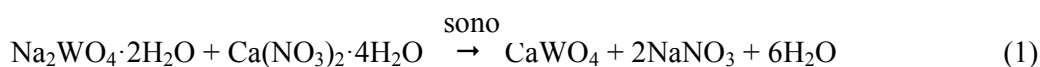
dodecylbenzenesulfonate (SDS) or cetyltrimethyl ammonium bromide (CTAB) was used. Their method needed surfactant-assisted solution, which is an expensive reagent and not environmentally friendly, and surfactants must be removed completely to obtain a pure product. This makes the synthetic step more complicated. Over the past few years, the sonochemical process has been applied to applications for synthesizing and customizing micro- and nano-structured inorganic and organic materials. The mechanism in this process occurred from acoustic cavitation (the formation, growth, and implosive collapse of bubbles in a liquid). This process has advantages such as uncomplicated steps, low energy consumption, time saving and high purity.

This study reports the fast synthesis of CaWO_4 microspheres almost monodispersed via the sonochemical route by using deionized (DI) water as intermediate solvent, which is environmentally friendly and has no assistance from surfactant or a template. The influence of different ultrasonic irradiation times, crystal structure, optical properties, and microstructure was investigated.

Experimental Procedure

Calcium nitrate tetrahydrate (99% $\text{Ca}(\text{NO}_3)_2 \cdot 4\text{H}_2\text{O}$) and sodium tungstate dihydrate (99% $\text{Na}_2\text{WO}_4 \cdot 2\text{H}_2\text{O}$) were purchased from Sigma–Aldrich Reagents Co., Ltd. and used without further purification. In a typical procedure, each 0.0167 mole of $\text{Ca}(\text{NO}_3)_2 \cdot 4\text{H}_2\text{O}$ and $\text{Na}_2\text{WO}_4 \cdot 2\text{H}_2\text{O}$ was dissolved separately in 50.00 ml of deionized (DI) water by stirring continuously until dissolved completely (transparent solution), without using an adjusted pH value of starting materials. After that, two solutions were added into the chamber and the ultrasonic probe (3 mm diameter; Ti-horn) was immersed with the frequency of pulsed ultrasound waves (conducted in the 2 s mode; and a pause in 1 s mode) at 20 kHz and 70

W/cm². The influence of different ultrasonic irradiation times was applied in the chamber containing mixed substrate solution for 1, 5, 15, and 30 min by the following reaction:



The white precipitate particles were washed with distilled water several times and then absolute ethanol before drying at 90°C for 24 hr. The X-ray diffraction (XRD) patterns of products were characterized by an X-ray diffractometer (D 8 Advance). The morphology of products was obtained by scanning electron microscope (SEM). The vibration mode of the bond in molecules was obtained from Fourier transform infrared (FT-IR spectrum Gx, Perkin Elmer, America) spectra. The sample was recorded in a wavelength range of between 400 and 4,000 cm⁻¹, and a Raman spectrophotometer (DXR smart Raman, Thermo scientific) with argon (Ar) laser recorded its wavelength range of between 200 and 1,000 cm⁻¹. The optical properties were investigated, and a portion of emission property was measured by a Fluorescence Spectrophotometer (Cary Eclipse model; Agilent Technologies, Varian, USA) with Xe lamp at room temperature, using an excitation wavelength (λ_{ex}) of 253 nm. A solid sample holder was used as a coated sample. The optical absorbance spectrum was examined by a UV-Vis spectrophotometer (T60, PG Instruments Limited) in the wavelength range of between 200 and 900 nm. The solution samples were prepared via mixing the powder samples in hydrogen peroxide to form a concentrated solution of 2 mM.

Results and discussion

a) Crystal structure

All the diffraction peaks in XRD patterns of the as-prepared CaWO₄ powders were synthesized by the sonochemical method at different ultrasonic irradiation times of 1, 5, 15 and 30 min, and could be indexed to a pure tetragonal scheelite structure ($a = b \neq c$, $\alpha = \beta = \gamma = 90^\circ$) with space group $I4_1/a$, when compare to the Joint Committee on Powder Diffraction

Standards (JCPDSs) card No.41-1431. Diffraction peaks corresponding to the secondary phase were undetected, and not a shift peak at different sonication times. In addition, peak intensities could be found to increase when ultrasound treatment time increases, as compared to the curves of four products that indicate better crystallization.¹¹ The percentage yield of the products obtained by this method was about 95%.

The Rietveld refinement method of XRD patterns was performed for CaWO_4 powders using the Fullprof program, as shown in Figure 1. This technique is based on the least-squares method,¹² where the theoretical peak patterns are adjusted upwards to converge with the result of measured patterns. It displays various advantages of typical quantitative analysis techniques, which comprise the use of pattern-fitting algorithms, and all lines of each crystallographic phase are considered explicitly. From structural refinement analysis, which provides various data on factors generally checked by quality algorithms of R-factors or chi-squared (χ^2), the difference between the measured and theoretical simulation patterns is considered a way to verify success of the refinement. The χ^2 value is the quality of fit, as the value distinguishes between theoretical simulations and the XRD pattern data result, which is more or less consistent, and this value should approach 1.

Upon inspection of the data, the tetragonal $I4_1/a$ space group and parameters (a, b, c, α , β , and γ) acquired from JCPDS Card No. 41-1431 were chosen for the initial refinement of the model. The fit of the XRD pattern data gave an χ^2 value of 1.27, 1.63, 2.11 and 2.34 for ultrasonic irradiation times of 1, 5, 15 and 30 min, respectively, which agreed well with acceptance for fitting the data. A large match of model intensities in peak variety, position and shape was assumed as correct from resulting refinement. This revealed that the selected space group and parameters were correct, and not that a completely pure phase of CaWO_4 was obtained at a 1 min sonication time, thus suggesting this method be used for a very short

time and utilized practically for synthesis of monodispersed CaWO_4 microspheres in field applications. The lattice parameters were calculated by using the Fullprof program, and those obtained were seen as a tetragonal unit cell type with a and c parameter values, as shown in Table 1. When comparing these lattice parameter values with JCPDS Card No. 41-1431, and lattice values from other various methods [3-4,6,13], good and acceptable agreement is found. However, the method in this study has more precise cell parameters than in other techniques, with the least deviation observed.

The Fourier transform infrared (FT-IR) spectra and Raman spectrophotometer were used to characterize the molecular structure of metal tungstate in order to verify the product structure. Typical CaWO_4 had a primitive cell of scheelite structure, which was characterized in its molecule consisting of $[\text{WO}_4]^{2-}$ molecular ionic groups (W metal in the tetrahedral site of O), with a strongly covalent W–O bond. The bonding between the $[\text{WO}_4]^{2-}$ molecular ionic groups and Ca^{2+} cations indicated loosely coupled bonds that were isolated from each other, while the Ca^{2+} was surrounded by eight oxygen ions. CaWO_4 presented a tetragonal structure of the symmetry, C_{4h} , at room temperature. The group theory calculation presented 26 different lattice vibrations for the CaWO_4 in a unit cell, where a zero wave vector can be described by the following equation [3,13-15].

$$\Gamma = 3A_g + 5A_u + 5B_g + 3B_u + 5E_g + 5E_u \quad (2)$$

while only infrared (IR), and Raman active modes are determined by the following equation [3,13-14].

$$\Gamma = 3A_g + 5B_g + 5E_g + 4A_u + 4E_u \quad (3)$$

All even vibrations (A_g , B_g and E_g) are Raman-active modes, while the odd modes (A_u and E_u) are active only in the infrared frequency range. Therefore, a 13 zone-center was expected in the Raman-active modes of CaWO_4 , as presented in the following equation [3,15].

$$\Gamma = 3A_g + 5B_g + 5E_g \quad (4)$$

From the literature, the vibrational modes found in the Raman spectra of CaWO_4 can be classified into two groups consisting of internal and external modes. Internal vibrations correspond to vibrations inside the $[\text{WO}_4]^{2-}$ molecular ionic group, which is considered as a stationary mass center. The lattice phonons or external vibrations are related to motion of the Ca^{2+} cations and rigidly molecular ionic $[\text{WO}_4]^{2-}$. In free space, $[\text{WO}_4]^{2-}$ tetrahedrons have a cubic point symmetry T_d [3,14-15], in which their vibrations are composed of four internal modes, $\nu_1(A_1)$, $\nu_2(E_1)$, $\nu_3(F_2)$ and $\nu_4(F_2)$, with one free rotation mode, $\nu_{\text{f.r.}}(F_1)$, and one translation mode (F_2) [3,14-15].

Raman spectra of CaWO_4 powders were obtained at different ultrasonic irradiation times (1, 5, 15 and 30 min), and operated in the wavenumber range of 100-1,000 cm^{-1} by using Ar laser as an excitation source, as shown in Figure 2. The graph shows six different modes of $\nu_1(A_g)$, $\nu_3(B_g)$, $\nu_3(E_g)$, $\nu_4(B_g)$, $\nu_2(A_g)$, and the free rotation of the z axis [$\nu_{\text{f.r.}}(A_g)$], occurring at about 914, 842, 798, 404, 333 and 212 cm^{-1} , respectively. The vibration modes in the Raman spectrum are A_g , B_g and E_g with peaks found mainly in internal modes, with W-O symmetric stretching vibration in molecular ionic $[\text{WO}_4]^{2-}$ [3].

FT-IR spectra of CaWO_4 powders obtained at different ultrasonic irradiation times (1, 5, 15 and 30 min), and operated at the wavenumber range of 400-4,000 cm^{-1} are shown in Figure 3. The FT-IR spectrum demonstrated a strong peak at about 802-803 cm^{-1} , which is in accordance with W-O asymmetric stretching vibration in molecular ionic $[\text{WO}_4]^{2-}$ [3], and weak W-O bending at about 430-460 cm^{-1} . Furthermore, O-H stretching and O-H bending

vibration of residual water were detected in powder products at 3,070-3,690 cm^{-1} and 1,620 cm^{-1} [3,16], respectively.

b) Optical Properties

The optical energy gap (E_g) of CaWO_4 powders was obtained from the calculation of their absorbance spectrum in UV-visible range by using Wood and Tauc's equation [3,16], which proposed the following:

$$\alpha h\nu = (h\nu - E_g)^n \quad (5)$$

where α is the optical absorption coefficient, h is the Planck constant, ν is the frequency of photon, E_g is the optical energy gap, and n is a constant that corresponds to the nature of an electronic transition. Transitions allowed directly, forbidden directly, allowed indirectly and forbidden indirectly are $n = 1/2, 3/2, 2$ and 3 , respectively. According to the literature, metal tungstate with a tetragonal scheelite structure has $n=1/2$ because its electronic transition is allowed directly [3,13,17]. The optical absorption coefficient, α , is calculated by using the following equation [13]

$$\alpha = -\ln T/d \quad (6)$$

where T is the optical transmittance and d is the optical path length through the cuvette. The E_g value was determined by extrapolating the straight linear portion of the relative graph between $(\alpha h\nu)^2$ and photon energy ($h\nu$) at an $h\nu$ value of 0. The $(\alpha h\nu)^2$ graph relative to the $h\nu$ value of CaWO_4 powders shows the E_g values at different ultrasonic irradiation times in Figure 4. Increased time makes an E_g value of 3.33, 3.36, 3.34 and 3.32 eV for different ultrasonic irradiation times of 1, 5, 15 and 30 min, respectively. It is noticeable that the E_g values differ slightly, due to the range of particle size varying insignificantly.

A fluorescence spectrophotometer was used to confirm the light emission spectrum of CaWO_4 powders. Figure 5 shows the fluorescence spectra of CaWO_4 microsphere powder samples obtained at different sonication times by using an excitation wavelength (λ_{ex}) of 253

nm. The broad peak emission positioned at a wavelength of around 420 nm indicates the direct transition gap of CaWO_4 microparticles. The blue light emission occurred from the ${}^1\text{T}_2 \rightarrow {}^1\text{A}_1$ transition intrinsic molecular anion $[\text{WO}_4]^{2-}$ group cluster [3]. The fluorescence spectrum discovered different intensities that could be the result of various particle sizes and crystallinity [11]. When comparing with the peak position of emission in bulk CaWO_4 , the tetragonal (scheelite) structure has a wavelength of 433 nm (2.87 eV) [18], where good acceptable agreement is found.

c) Microstructure

Figure 6(a) shows the products prepared from mixing substance solution, then leaving it until precipitation occurs (without ultrasonic irradiation). The morphology obtained varied greatly, with broad size distribution. The particle sizes were difficult to measure, due to the random aggregation of mixed powder that appeared between spherical particles and spread nanoparticles. Figures 6(b)-(h) show CaWO_4 powders synthesized under different ultrasonic irradiations. Near spherical shape and narrow particle size distribution, with a micron size of the powders, were observed clearly at a radiation time of 1 min [Figure 6(b)]. The average size of the microsphere was about $7.59 \pm 1.20 \mu\text{m}$. When enlarging the image of only one particle [Figure 6(c)], the texture of microspheres was composed of aggregated small nanoparticles, with an average particle size of $52.87 \pm 1.39 \text{ nm}$. The mono size with spherical shape was observed clearly at a sonication time of 5 min [Figure 6(d)]. The average diameter of the spheres increased to about $11.20 \pm 1.07 \mu\text{m}$. Furthermore, the morphology obtained at the sonication time of 15 min was a mixture of small and large microsphere particles and rarely spherical-shaped ones [Figure 6(e)]. Evidently, the neck between the microsphere particles was observed from this condition. Figure 6(f) shows expansion of the neck with melted nanoparticles on the surface area. When the reaction time increased to 30 min, a very rough surface of microparticles was obtained, as shown in Figure 6(g).

Furthermore, neck point breaking is shown between microspheres, with small clusters of particles that had broken off [Figure 6(h)].

Possible growth process and effect of ultrasonic irradiation time

Figure 7 shows a schematic illustration of the growth process of monodispersed CaWO_4 microspheres via the sonochemical process by ultrasonic time-dependent experiments. The precursor solid (as the calcium and tungstate ion source) was hydrolyzed immediately in DI water as solvent in order to create Ca^{2+} and WO_4^{2-} ions. Additionally, Ca^{2+} and WO_4^{2-} species were attracted at the initial formation stage by electrostatic interaction, and formed numerous CaWO_4 nuclei. Subsequently, the mixed solution was irradiated with high-intensity ultrasound (70 W/cm^2 , 20 kHz). Precipitation in the liquid-solid heterogeneous system was accelerated completely by ultrasonic irradiation, which resulted from the acoustic cavitation process (the formation, growth, and implosive collapse of bubbles in a liquid). At the initial state (0 min), primary nanoparticles appeared and tended to aggregate into soft nanoparticle clusters in order to reduce each other's surface energy. With the ultrasonic time at 1 min, CaWO_4 microspheres were assembled by unstable nanoparticle cluster orientation. As seen, each microsphere consisted of numerous tightly packed nanospheres resulting in rough surfaces. It is known that collapsing bubbles create OH^\cdot and H^\cdot radical species via the sonolysis of water in an aqueous solution, and preferably yield formation of H_2O_2 , H_2O etc. From previous observation [19], hydroxyl groups ($-\text{OH}$) were produced from radical species that prefer to react with oxygen ions, and also, H_2O_2 was likely to decompose on the surface of metal oxide particles. These hydroxyl groups on the surface of CaWO_4 nanoparticles promote self-attachment between unstable nanoparticles, thus resulting in aggregation of single microspheres on a surface consisting of nanospheres. This study considered that high-intensity ultrasound irradiation also plays an important role in the formation of products

leading to the microspherization process [20-21]. The result of this study is similar to that of Xu et al. [21,23], in which prepared polysaccharide-based and chitosan microspheres used the single-step sonochemical method. However, the morphology of CaWO_4 in this work was quite different from that reported by Yang et.al [22]. The difference in morphology might be attributed to varied synthesis parameters such as ultrasonic frequency, pH value and ultrasonication mode [22]. At 5 min sonication time, stable monodispersed microspheres would steadily aggregate in mostly narrow particle size distribution. The diameter of these particles became larger simultaneously to an unsurpassable critical size limit, of which the microsphere particles in this work were about $11.20 \pm 1.07 \mu\text{m}$. The critical size limit of these particles strongly depends on many factors such as ultrasonic frequency, velocity of interparticle collisions and shock waves generated by cavitation in liquids irradiated with ultrasound [24]. These shock waves can induce physical effect, especially by increasing mass transport. Shock waves through the microsphere particles can expedite and drive microparticles suspended in liquid into one another, and the impact velocity of these collisions between particles can be estimated at around one hundred meters per second [23]. This physical effect causes changes in surface composition, distribution of particle size and particle morphology [23]. Additionally, a short-lived localized hot-spot that produces enormous volumes of temperature at $\sim 5,000 \text{ K}$, pressure of $\sim 1,000 \text{ atm}$ and heating and cooling rates of $> 10^{10} \text{ K/s}$ can be generated during cavitations [24-25]. As a result, necking occurred at 15 min between microsphere particles, which was similar to the initial stage of the solid-state sintering process. It is believed that this heat energy occurrence can make surface diffusion, as the melting point started from the surface area of nanoparticles on the microsphere particles. Surface diffusion is a typical mass transport in the sintering mechanism that produces surface smoothing, particle joining, grain boundary formation, neck growth, and pore rounding [26-27]. However, volume shrinkage and densification was not

found, due to the sonochemical method generating local thermal energy, which is different from thermal energy of the sintering process. When increasing the sonication time to 30 min, the necking and unsmooth surface broke into a large number of particle scraps, with no single monodispersed microspheres. As a result, impact from high speed microjets on the surface led to the phenomena of morphological transformations, including particles breaking and erosion of material [23, 28]. Furthermore, the average particle sizes, as a function of ultrasonic irradiation time, are plotted in Figure 8. Increasing time gradually increases microsphere particles to an average size of $11.20 \pm 1.07 \mu\text{m}$ and narrow standard deviation at 5 min, which is suitable for producing uniformed spherical morphology. A broad size deviation was observed as the time increased to 15 and 30 min, due to difficulty in finding the particle sizes after necking and microsphere breakage. Based on the results obtained at different ultrasonic times, formation of the monodispersed CaWO_4 microsphere can be controlled easily by only one single parameter in a simple sonochemical process.

Conclusion

Nearly monodispersed CaWO_4 microspheres were accomplished via the sonochemical process by using deionized (DI) water as intermediate solvent at an ultrasonic irradiation time of 5 min. XRD results exhibited CaWO_4 powders as a tetragonal scheelite structure. SEM images showed the morphology as monodispersed CaWO_4 microspheres of $11.20 \pm 1.07 \mu\text{m}$. The growth mechanism was performed carefully by brief ultrasonic time-dependence. The fluorescence spectra of CaWO_4 nanoparticles obtained a blue light that was emitted at a wavelength of around 420 nm. The E_g values obtained results of the absorbance spectrum at 3.32 - 3.36 eV. This synthesized method for monodispersed CaWO_4 microspheres presents advantages such as uncomplicated steps, low energy consumption, high purity, time-saving and suitable application.

Acknowledgments

This work was supported by the Thailand Research Fund (TRF) under Grant No. BRG5680006. The authors would like to thank Dr. Jakrapong Kaewkhao for the support of Photoluminescence measurement.

References

1. L. Sun, M. Cao, Y. Wang, G. Sun and C. Hu, *J. Cryst. Growth.*, 2006, **289**, 231-235.
2. J. Liu, Q. Wu and Y. Ding, *J. Cryst. Growth.*, 2005, **279**, 410–414.
3. T. Thongtem, S. Kungwankunakorn, B. Kuntalue, A. Phuruangrat and S. Thongtem, *J. Alloy Compd.*, 2010, **506**, 475–481.
4. Y. Tian, Y. Liu, R. Hua, L. Na and B. Chen, *Mater. Res. Bull.*, 2012, **47**, 59–62.
5. Y. Wang, J. Ma, J. Tao, X. Zhu, J. Zhou, Z. Zhao, L. Xie and H. Tian, *Mater. Lett.*, 2006, **60**, 291 – 293.
6. S.J. Chen, J. Li, X.T. Chen, Jian-Ming Hong, Ziling Xue, and Xiao-Zeng You, *J. Cryst. Growth.*, 2003, **253**, 361–365.
7. P. Parhi, T. N. Karthik and V. Manivannan, *J. Alloy Compd.*, 2008, **465**, 380-386.
8. H. Pan, M. Hojamberdiev and G. Zhu, *J. Mater. Sci.*, 2012, **47**, 746-753.
9. Q. Zhang, W. T. Yao, X. Chen, L. Zhu, Y. Fu, G. Zhang, L. Sheng and S. H. Yu, *Cryst. Growth Des.*, 2007, **7**, 1423-1431.
10. G. Jia, D. Dong, C. Song, L. Li, C. Huang and C. Zhang, *Mater Lett.*, 2014, **120**, 251-254.
11. J. Geng, J. J. Zhu and H. Y. Chen, *Cryst. Growth Des.*, 2006, **6**, 321-326.
12. J.E. Post and D.L. Bish, *Am. Mineral.*, 1993, **78**, 932-940.
13. S. Vidya, S. Solomon and J. K. Thomas, *J. Electron. Mater.*, 2013, **42**, 129-137.
14. J. C. Sczancoski, L. S. Cavalcante, M. R. Joya, J. W. M. Espinosa, P. S. Pizani, J. A. Varela and E. Longo, *J. Colloid Interf. Sci.*, 2009, **330**, 227-236.

15. L. S. Cavalcante, J. C. Sczancoski, J. W. M. Espinosa, J. A. Varela, P. S. Pizani and E. Longo, *J. Alloy Compd.*, 2009, **474**, 195-200.
16. J. Liao, B. Qiu, H. Wen and W. You, *Opt. Mater.*, 2009, **31**, 1513-1516.
17. J. C. Sczancoski, M. D. R. Bomio, L. S. Cavalcante, M. R. Joya, P. S. Pizani, J. A. Varela, E. Longo, M. S. Li and J. A. Andrés, *J. Phys. Chem. C.*, 2009, **113**, 5812-5822.
18. M. J. Weber and W. M. Yen, *Inorganic phosphors: Compositions, Preparation, and Optical Properties*. 1932, 194.
19. S. J. Chang, W. S. Liao, C. J. Ciou, J. T. Lee and C. C. Li, *J. Colloid. Interf Sci.*, 2009, **329**, 300–305.
20. N. Skirtenko, T. Tzanov, A. Gedanken and S. Rahimipour, *Chem. Eur. J.*, 2010, **16**, 562 – 567.
21. R. Silva, H. Ferreira and A. Cavaco-Paulo, *Biomacromolecules*, 2011, **12**, 3353–3368.
22. L. Yang, Y. Wang, Y. Wang, X. Wang and G. Han, *Adv. Powder. Technol.*, 2013, **24**, 721–726.
23. X. Hangxun, B. W. Zeiger and K. S. Suslick, *Chem. Soc. Rev.*, 2013, **42**, 2555-2567.
24. K. S. Suslick and S. J. Dockeycz, *Adv. Sonochem.*, **1990**, *1*, 197-230.
25. K. S. Suslick, *Sci. Am*, 1989, 80-86.
26. J. S. Reed, *Principles of ceramics processing*, A Wiley-Interscience Publication, 1995, 594-606.
27. S-J. L. Kang, *Sintering: Densification, Grain Growth, and Microstructure*, 2005.
28. L. Zhang, V. Belova, H. Wang, W. Dong and H. Möhwald, *Chem. Mater.*, 2014, **26**, 2244–2248.

Table Headings

Table 1 The refinement values of CaWO₄ powders and comparison with the lattice parameters from other methods

Figure Legends

- Figure 1. Rietveld analysis of XRD patterns of CaWO₄ powders synthesized by the sonochemical method at different ultrasonic irradiation times.
- Figure 2. Raman spectra of CaWO₄ powders obtained at different ultrasonic irradiation times.
- Figure 3. FT-IR spectra of CaWO₄ powders obtained at different ultrasonic irradiation times.
- Figure 4. Relative graph of the $(\alpha h\nu)^2$ with $h\nu$ (eV) of CaWO₄ powders.
- Figure 5. Fluorescence spectrum of CaWO₄ powders obtained at different ultrasonic irradiation times.
- Figure 6. SEM images of CaWO₄ powder obtained, (a) without ultrasonic irradiation, and produced from ultrasonic irradiation, (b) at 1 min, (c) with only one enlarged microspherical particle showing a surface with aggregated primary nanoparticles (inset image), (d) at 5 min, (e) at 15 min, (f) with the neck between microsphere particles at 15 min, (g) at 30 min, and (h) microspherical breaking at 30 min.
- Figure 7. Schematic illustration of the growth process of monodispersed CaWO₄ microspheres via the sonochemical process of ultrasonic irradiation time - dependent experiments.
- Figure 8. Plotting of average particle sizes with ultrasonic irradiation time.

Table 1. The refinement values of CaWO_4 powders and comparison with the lattice parameters from other methods

Methods	time	Lattice parameters (\AA)		χ^2	Ref.
		A	c		
Sonochemical	1 min	5.238 ± 0.002	11.389 ± 0.003	1.27	This work
Sonochemical	5 min	5.243 ± 0.001	11.370 ± 0.004	1.63	This work
Sonochemical	15 min	5.235 ± 0.001	11.369 ± 0.003	2.11	This work
Sonochemical	30 min	5.240 ± 0.001	11.379 ± 0.005	2.34	This work
Hydrothermal	8 h	5.252	11.388	-	8
Solvothermal	-	5.46	12.04	-	9

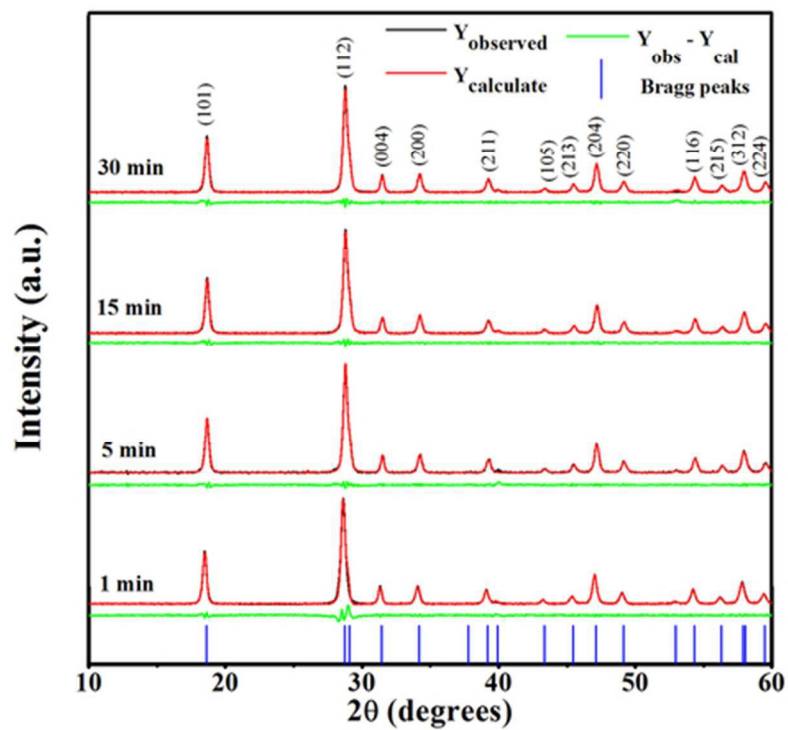


Figure 1. Rietveld analysis of XRD patterns of CaWO₄ powders synthesized by the sonochemical method at different ultrasonic irradiation times.
51x39mm (300 x 300 DPI)

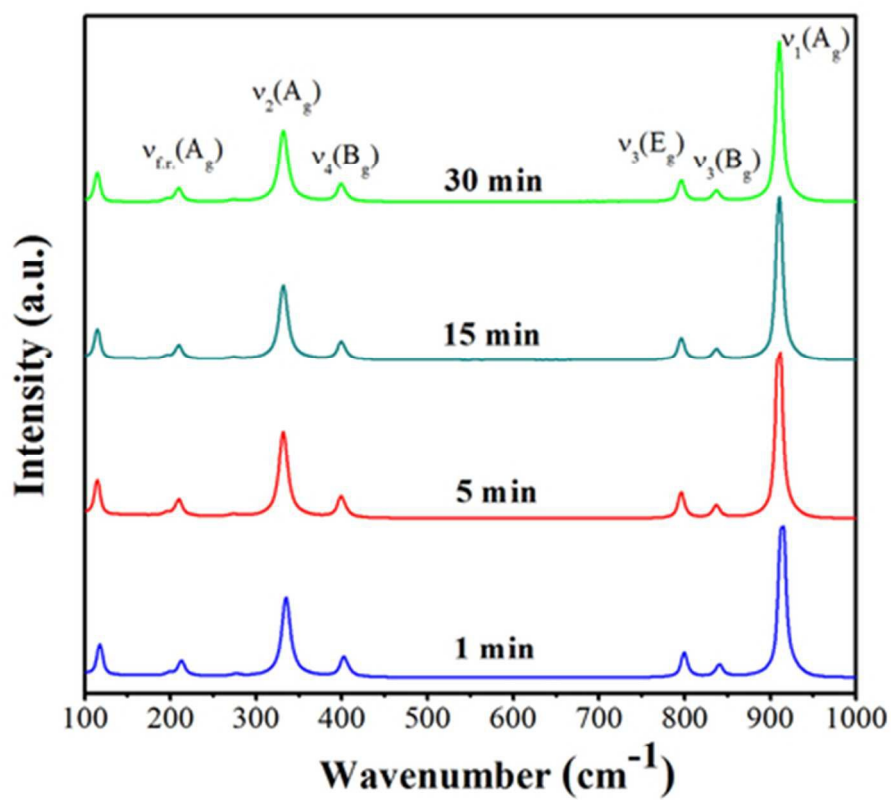


Figure 2. Raman spectra of CaWO₄ powders obtained at different ultrasonic irradiation times.
42x37mm (300 x 300 DPI)

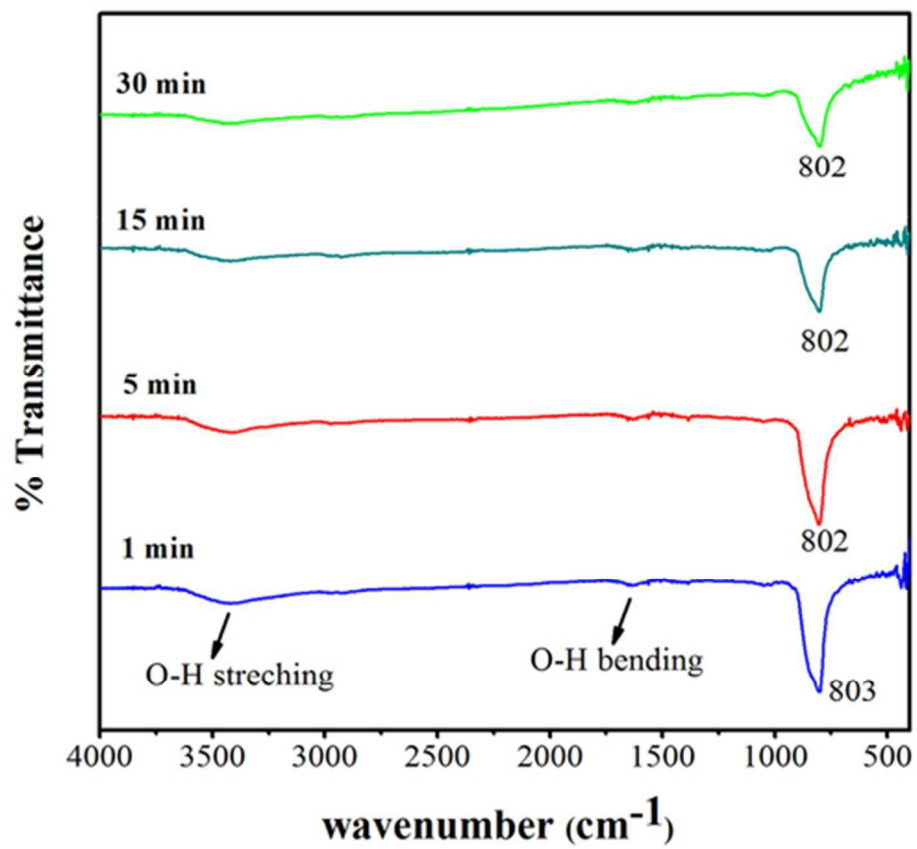


Figure 3. FT-IR spectra of CaWO₄ powders obtained at different ultrasonic irradiation times. 45x41mm (300 x 300 DPI)

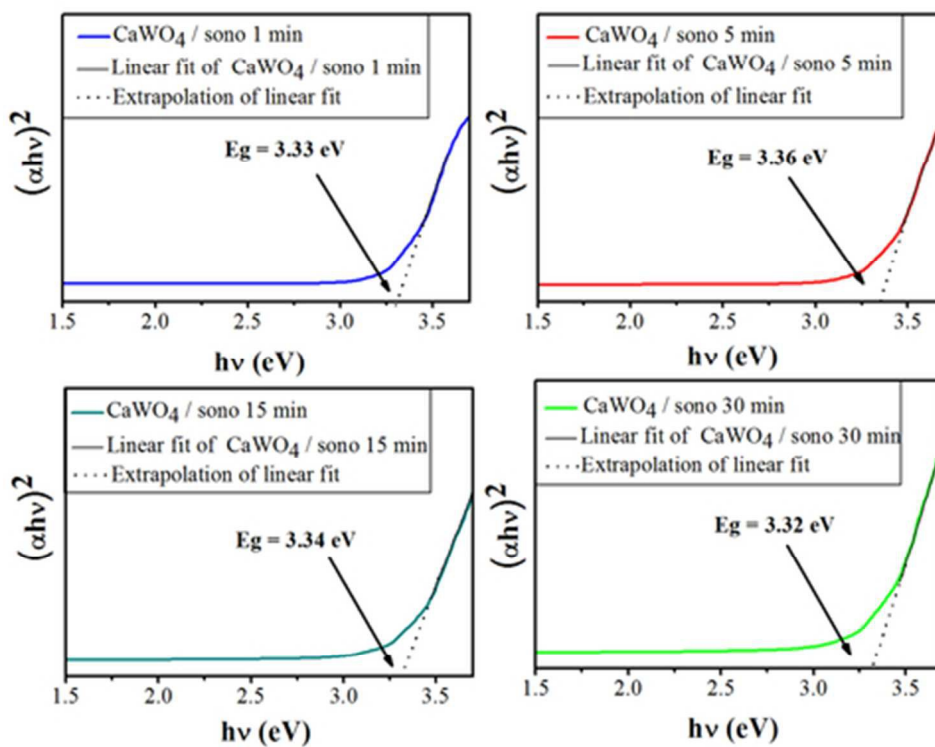


Figure 4. Relative graph of the $(\alpha h\nu)^2$ with $h\nu$ (eV) of CaWO_4 powders. 42x33mm (300 x 300 DPI)

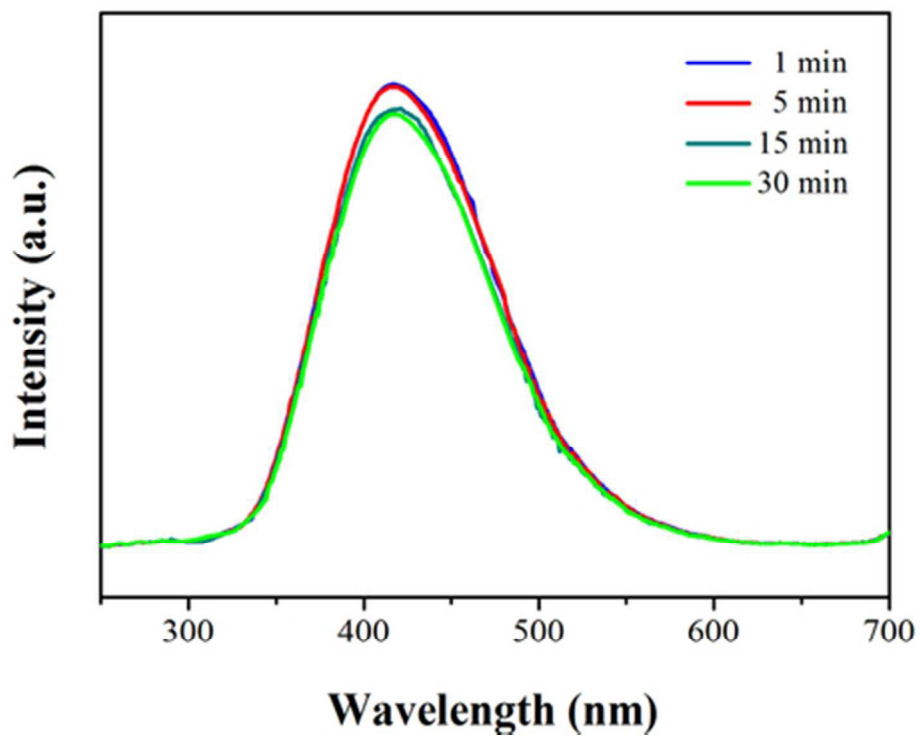


Figure 5. Fluorescence spectrum of CaWO₄ powders obtained at different ultrasonic irradiation times.
42x32mm (300 x 300 DPI)

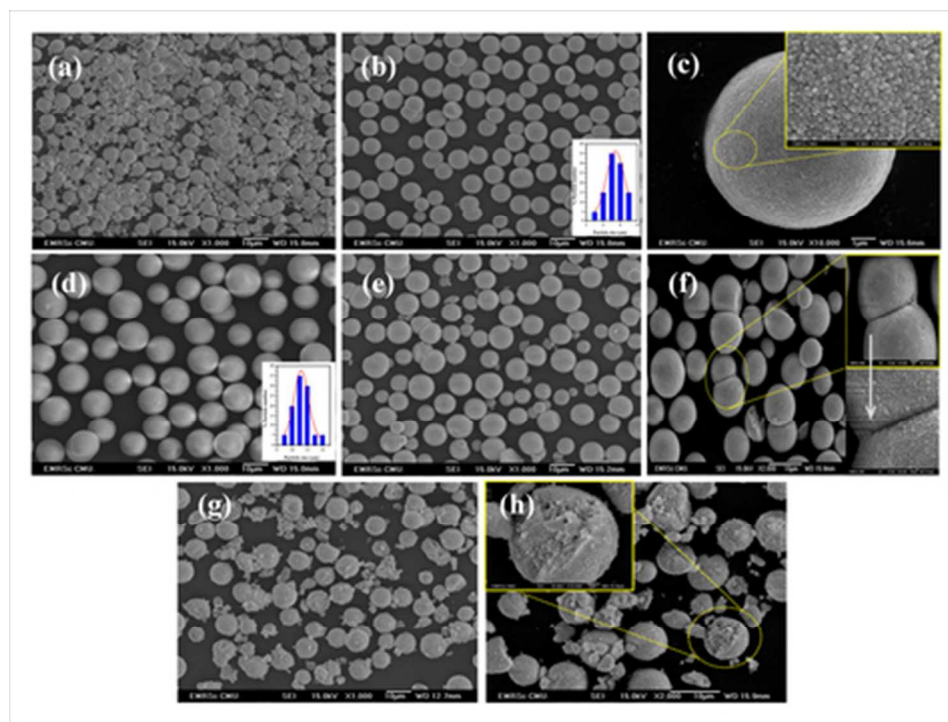


Figure 6. SEM images of CaWO_4 powder obtained, (a) without ultrasonic irradiation, and produced from ultrasonic irradiation, (b) at 1 min, (c) with only one enlarged microspherical particle showing a surface with aggregated primary nanoparticles (inset image), (d) at 5 min, (e) at 15 min, (f) with the neck between microspherical particles at 15 min, (g) at 30 min, and (h) microspherical breaking at 30 min. 40x30mm (300 x 300 DPI)

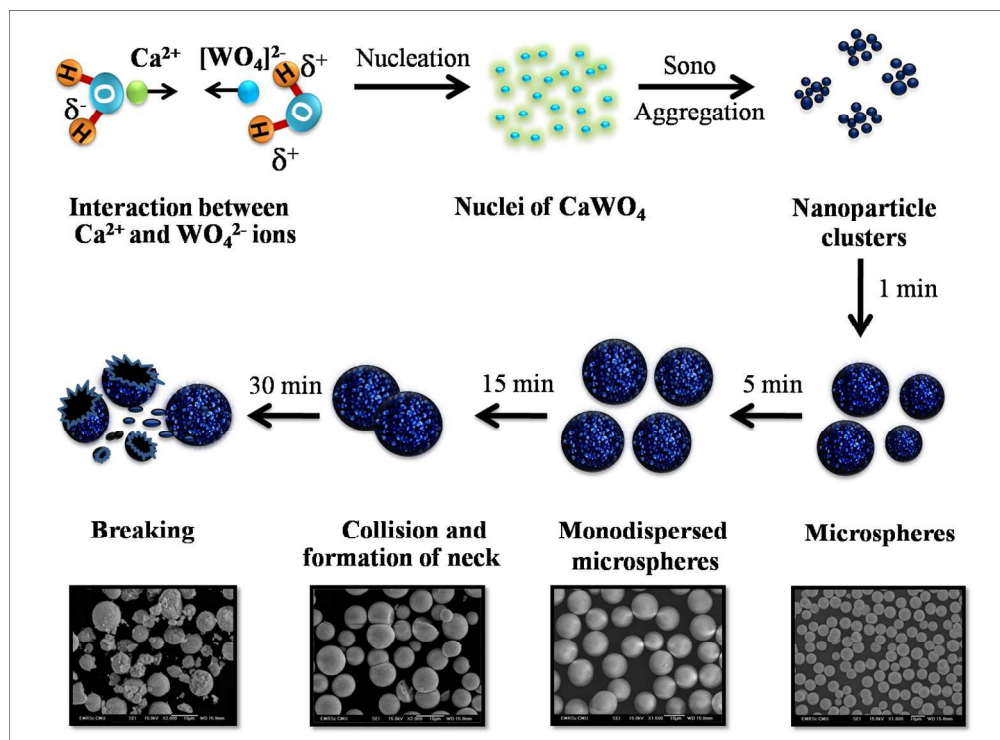


Figure 7. Schematic illustration of the growth process of monodispersed CaWO_4 microspheres via the sonochemical process of ultrasonic irradiation time - dependent experiments.
272x200mm (150 x 150 DPI)

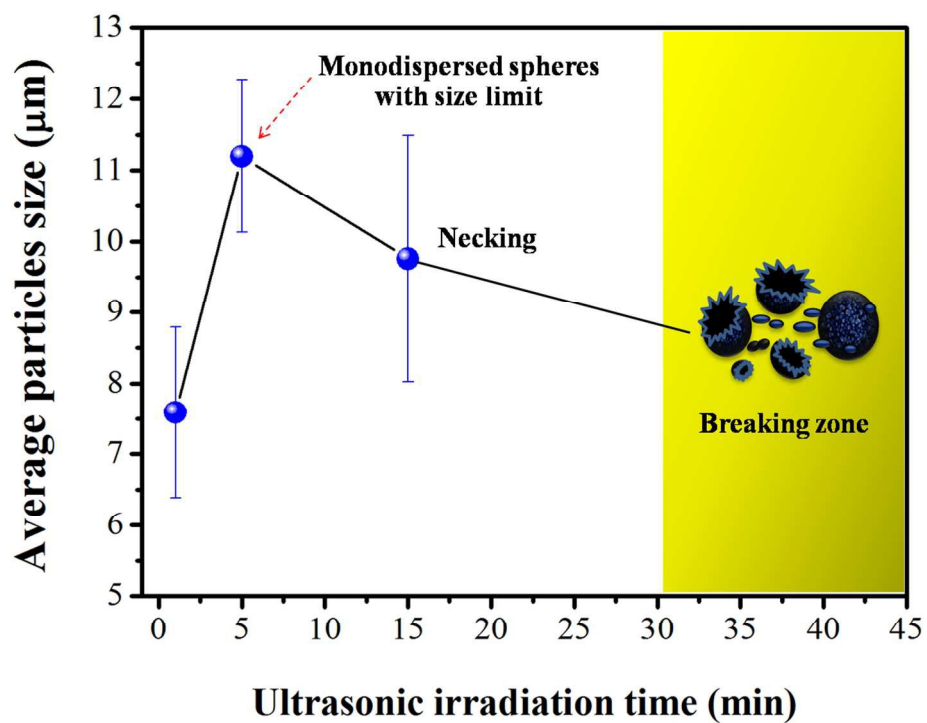


Figure 8. Plotting of average particle sizes with ultrasonic irradiation time.
225x168mm (150 x 150 DPI)